



The Afterglow and Ulig Host Galaxy of the Dark Short Grb 120804a

Citation

Berger, E., B. A. Zauderer, A. Levan, R. Margutti, T. Laskar, W. Fong, V. Mangano, et al. 2013. The Afterglow and Ulig Host Galaxy of the Dark Short Grb 120804a. *The Astrophysical Journal* 765, no. 2: 121. doi:10.1088/0004-637x/765/2/121.

Published Version

doi:10.1088/0004-637x/765/2/121

Permanent link

<http://nrs.harvard.edu/urn-3:HUL.InstRepos:30456065>

Terms of Use

This article was downloaded from Harvard University's DASH repository, and is made available under the terms and conditions applicable to Open Access Policy Articles, as set forth at <http://nrs.harvard.edu/urn-3:HUL.InstRepos:dash.current.terms-of-use#OAP>

Share Your Story

The Harvard community has made this article openly available.
Please share how this access benefits you. [Submit a story](#).

[Accessibility](#)

THE AFTERGLOW AND ULIRG HOST GALAXY OF THE DARK SHORT GRB 120804A

E. BERGER¹, B. A. ZAUDERER¹, A. LEVAN², R. MARGUTTI¹, T. LASKAR¹, W. FONG¹, V. MANGANO³, D. B. FOX⁴,
R. L. TUNNICLIFFE², R. CHORNOCK¹, N. R. TANVIR⁵, K. M. MENTEN⁶, J. HJORTH⁷, K. ROTH⁸, AND T. J. DUPUY¹

Draft version September 26, 2012

ABSTRACT

We present the optical discovery and sub-arcsecond optical and X-ray localization of the afterglow of the short GRB 120804A, as well as optical, near-IR, and radio detections of its host galaxy. X-ray observations with *Swift*/XRT, *Chandra*, and *XMM-Newton* extending to $\delta t \approx 19$ d reveal a single power law decline. The optical afterglow is faint and comparison to the X-ray flux indicates that GRB 120804A is “dark”, with a rest-frame extinction of $A_V^{\text{host}} \approx 2.5$ mag (at $z \approx 1.3$). The intrinsic neutral hydrogen column density inferred from the X-ray spectrum, $N_{\text{H,int}}(z = 1.3) \approx 2 \times 10^{22} \text{ cm}^{-2}$, is commensurate with the large extinction. The host galaxy exhibits red optical/near-IR colors. Equally important, JVLA observations at ≈ 0.9 –11 d reveal a constant flux density of $F_\nu(5.8 \text{ GHz}) = 35 \pm 4 \mu\text{Jy}$ and an optically-thin spectrum, unprecedented for GRB afterglows, but suggestive instead of emission from the host galaxy. The optical/near-IR and radio fluxes are well fit with the scaled spectral energy distribution of the local ultra-luminous infrared galaxy (ULIRG) Arp 220 at $z \approx 1.3$, with a resulting star formation rate of $\approx 300 M_\odot \text{ yr}^{-1}$. The inferred extinction and small projected offset (2.2 ± 1.2 kpc) are also consistent with the ULIRG scenario, as is the presence of a companion galaxy at a separation of about 11 kpc. The limits on radio afterglow emission, in conjunction with the observed X-ray and optical emission, require a circumburst density of $n \sim 10^{-3} \text{ cm}^{-3}$ an isotropic-equivalent energy scale of $E_{\gamma,\text{iso}} \approx E_{\text{K,iso}} \approx 7 \times 10^{51} \text{ erg}$, and a jet opening angle of $\theta_j \gtrsim 8^\circ$. The expected fraction of luminous infrared galaxies in the short GRB host sample is ~ 0.01 –0.3 (for pure stellar mass and star formation weighting, respectively). Thus, the observed fraction of 2 events in about 25 hosts (GRBs 120804A and 100206A), provides additional support to our previous conclusion that short GRBs track both stellar mass and star formation activity.

Subject headings: gamma rays: bursts

1. INTRODUCTION

Short-duration gamma-ray bursts (GRBs) occur in a wide range of environments that include elliptical and star forming galaxies in the field and in clusters (e.g., Berger 2011 and references therein). These galaxies have redshifts of $z \approx 0.1$ to $\gtrsim 1$ (Berger et al. 2007; Rowlinson et al. 2010), star formation rates of $\text{SFR} \lesssim 0.01$ to $\approx 40 M_\odot \text{ yr}^{-1}$ (Berger 2009; Perley et al. 2011a), and stellar masses of $M_* \approx 10^9$ – $4 \times 10^{11} M_\odot$ (Leibler & Berger 2010). These properties are suggestive of a progenitor population that tracks both stellar mass and star formation activity (though with a significant delay of ~ 0.3 Gyr; Leibler & Berger 2010), in agreement with the popular compact object coalescence model (e.g., Eichler et al. 1989; Narayan et al. 1992).

In a similar vein, short GRBs also exhibit a range of explosion properties, with isotropic-equivalent energies of $E_{\gamma,\text{iso}} \sim E_{\text{K,iso}} \sim 10^{49}$ – 10^{52} erg (Berger 2007; Nakar 2007; Nysewander et al. 2009), jet opening angles of $\theta_j \approx$ few to $\gtrsim 20$ deg in a few cases (Burrows et al. 2006; Grupe et al.

2006; Soderberg et al. 2006; Watson et al. 2006; Fong et al. 2012), and circumburst densities of $n \lesssim 1 \text{ cm}^{-3}$ (Berger et al. 2005; Soderberg et al. 2006; Fong et al. 2012). The distribution of opening angles is of particular importance since it impacts the true energy scale and event rate. To date, all measurements or limits on θ_j have relied on X-ray observations thanks to the relative brightness and high detection fraction of the afterglow in the X-ray band compared to the optical and radio bands (Nysewander et al. 2009; Berger 2010).

Here we present the optical discovery and sub-arcsecond localization of the optical and X-ray afterglow of the short GRB 120804A, as well as optical, near-IR, and radio detections of its host galaxy. The afterglow data constrain the burst properties ($E_{\text{K,iso}}$, θ_j , n). The host galaxy observations identify it as an ultra-luminous infrared galaxy (ULIRG) at a photometric redshift of $z \approx 1.3$, making GRB 120804A one of the most distant short bursts known to date. This is the first ULIRG host in the short GRB sample, exceeding even the luminous infrared galaxy (LIRG) likely host of GRB 100206A (Perley et al. 2011a). We present the afterglow and host galaxy observations in §2, extract the explosion properties in §3, and determine the host galaxy photometric redshift and properties in §4. Throughout the paper we report magnitudes in the AB system (unless otherwise noted), use a Galactic extinction value of $E(B-V) \approx 0.204$ mag (Schlafly & Finkbeiner 2011), and employ the standard cosmological parameters: $H_0 = 71 \text{ km s}^{-1} \text{ Mpc}^{-1}$, $\Omega_\Lambda = 0.73$, and $\Omega_M = 0.27$.

2. OBSERVATIONS AND ANALYSIS

GRB 120804A was discovered with the *Swift* Burst Alert Telescope (BAT) on 2012 August 4 at 00:55:47.8 UT (Baumgartner et al. 2012), and was also detected with Konus-

¹ Harvard-Smithsonian Center for Astrophysics, 60 Garden Street, Cambridge, MA 02138, USA

² Department of Physics, University of Warwick, Coventry, CV4 7AL, UK

³ INAF, Istituto di Astrofisica Spaziale e Fisica Cosmica, Via U. La Malfa 153, I-90146 Palermo, Italy

⁴ Department of Astronomy and Astrophysics, The Pennsylvania State University, 525 Davey Lab, University Park, PA 16802, USA

⁵ Department of Physics and Astronomy, University of Leicester, University Road, Leicester LE1 7RH, UK

⁶ Max-Planck-Institut für Radioastronomie, Auf dem Hügel 69, 53121, Bonn, Germany

⁷ Dark Cosmology Centre, Niels Bohr Institute, University of Copenhagen, Juliane Maries Vej 30, DK-2100 Copenhagen Ø, Denmark

⁸ Gemini Observatory, 670 North Aohoku Place, Hilo, HI 96720, USA

WIND (Sakamoto et al. 2012). The burst duration is $T_{90} = 0.81 \pm 0.08$ s (15–350 keV) with a fluence of $F_{\gamma} = (8.8 \pm 0.5) \times 10^{-7}$ erg cm $^{-2}$ (15–150 keV) and $(1.45 \pm 0.30) \times 10^{-6}$ erg cm $^{-2}$ (15–1000 keV). A joint analysis of the BAT and Konus-WIND data indicates a peak energy of $E_p = 135^{+66}_{-29}$ keV (Sakamoto et al. 2012). The spectral lags are 16 ± 12 ms (15–25 to 50–100 keV) and -5 ± 6 ms (25–50 to 100–350 keV), typical of short GRBs (Norris et al. 2012).

Swift/X-ray Telescope (XRT) observations commenced about 78 s after the burst and led to the identification of a fading source, located at RA=15^h35^m47.51^s, Dec=−28°46′56.9″ with an uncertainty of 1.4″ radius (90% containment, UVOT-enhanced; Osborne et al. 2012). Observations with the UV/Optical Telescope (UVOT) began about 97 s after the burst, but no counterpart was detected to a 3σ limit of $\gtrsim 21.4$ mag in the white filter (at $\delta t \approx 97–247$ s; Chester & Lien 2012). Optical and near-IR observations with GROND starting at $\delta t \approx 1.5$ hr also led to non-detections with $\gtrsim 22$ mag (*griz*) and $\gtrsim 20.6$ mag (*J*-band; Sudilovsky et al. 2012).

2.1. X-ray Observations

We analyze the *Swift*/XRT data using the HEASOFT package (v6.11) and latest calibration files with the standard filtering and screening criteria. We generate the 0.3–10 keV count-rate light curve following the procedure described in Margutti et al. (2012), with a re-binning scheme that ensures a minimum signal-to-noise ratio of 4 for each temporal bin. The data comprise 33 s ($\delta t \approx 97–130$ s) in Windowed Timing (WT) mode, and 18 ks in Photon Counting (PC) mode ($\delta t \approx 150–6 \times 10^4$ s).

We fit the time-averaged WT spectrum with an absorbed power-law model (*tbabs* \times *ztbabs* \times *pow* in *Xspec*) using a Galactic neutral hydrogen column density of $N_{\text{H,MW}} \approx 9.3 \times 10^{20}$ cm $^{-2}$ (Kalberla et al. 2005). The resulting spectral photon index is $\Gamma = (2.5 \pm 0.3)$ and the excess neutral hydrogen column density is $N_{\text{H,int}} = (3.5 \pm 1.1) \times 10^{21}$ cm $^{-2}$ at $z = 0$ (C–stat = 92 for 122 degrees of freedom; uncertainties are 1σ). From the time-averaged PC spectrum we infer $\Gamma = (2.1 \pm 0.1)$ and $N_{\text{H,int}} = (3.2 \pm 0.5) \times 10^{21}$ cm $^{-2}$ at $z = 0$ (C–stat = 283 for 316 degrees of freedom). We adopt the latter value of $N_{\text{H,int}}$ in the time-resolved spectral analysis, designed to account for the source spectral evolution and the resulting count-to-flux conversion factor (Margutti et al. 2012). The uncertainties arising from the flux calibration are properly propagated in the unabsorbed 0.3–10 keV flux light curve. We note that at $z \approx 1.3$ (see §4) the best-fit parameters are $\Gamma \approx 1.9$ and the intrinsic neutral hydrogen column density is $N_{\text{H,int}} \approx 2 \times 10^{22}$ cm $^{-2}$.

We also analyze a *Chandra* ACIS-S observation obtained on 2012 August 13.45 UT ($\delta t \approx 9.41$ d) with a total exposure time of 19.8 ks (PI: Troja; Troja et al. 2012). The X-ray afterglow is detected with a significance of about 13σ at a count rate of 1.6 ± 0.3 cps in the 0.5–8 keV range. Adopting the best-fit spectral parameters from the XRT analysis this translates to an unabsorbed 0.3–10 keV flux of $(2.8 \pm 0.5) \times 10^{-14}$ erg s $^{-1}$ cm $^{-2}$.

We further obtained an XMM-*Newton* observation on 2012 August 22.91 UT ($\delta t \approx 18.9$ d; PI: Margutti) to search for the signature of a jet break at late time. We analyze the EPIC data with the XMM Science Analysis System (SAS v11.0.0), selecting events with PATTERN ≤ 12 for the MOS cameras, PATTERN ≤ 4 for the pn camera, and FLAG = 0 for both. To reduce the contamination by soft proton flares, we screen

the original event files using a sigma-clipping algorithm. The remaining good science time is 29.5 ks for MOS1 and MOS2, and 25.5 ks for pn. The X-ray afterglow is detected in the MOS1 and MOS2 images with $(1.0 \pm 0.3) \times 10^{-3}$ cps (0.2–10 keV) and in the pn image at the with $(4.3 \pm 0.7) \times 10^{-3}$ cps (0.2–10 keV). We perform spectral analysis using the *evselect* tool, with the response files generated with the *rmfgen* and *arfgen* tools. The resulting inter-calibration factor of MOS1 and MOS2 relative to pn is 0.9–1.1. We adopt the value of $N_{\text{H,int}}$ from the XRT analysis, leading to a pn unabsorbed 0.3–10 keV flux of $(2.4 \pm 0.5) \times 10^{-14}$ erg s $^{-1}$ cm $^{-2}$.

2.2. Optical Afterglow Discovery and Relative X-ray Astrometry

We obtained two epochs of *i*-band imaging with the Gemini Multi-Object Spectrograph (GMOS; Hook et al. 2004) on the Gemini-North 8-m telescope on 2012 August 4.27 and 7.30 UT ($\delta t \approx 0.23$ d and ≈ 3.26 d, respectively). The observations consisted of 1980 s and 2880 s, respectively, in 0.65″ seeing. We process the data using the *gemini* package in IRAF, and perform photometry using a zero-point of 28.46 ± 0.10 mag measured on the nights of August 2–8 UT. We perform digital image subtraction of the two epochs with the ISIS package (Alard 2000), and recover a fading source with $m_i = 26.2 \pm 0.2$ AB mag (with an additional systematic uncertainty of ± 0.1 mag due to the zero-point uncertainty). We consider this source to be the optical afterglow of GRB 120804A. Corrected for Galactic extinction the resulting flux density is $F_{\nu} = 0.17 \pm 0.05$ μ Jy. Images of the two epochs and the resulting subtraction are shown in Figure 1.

We determine the absolute position of the afterglow by astrometrically matching the images to the 2MASS reference frame using 45 common sources. The resulting astrometric uncertainty is 0.15″ in each coordinate. The afterglow position in the residual image is RA=15^h35^m47.479^s, Dec=−28°46′56.17″ (J2000), with a centroid uncertainty of about 0.05″ in each coordinate.

To locate the *Chandra* X-ray afterglow on the optical images we perform differential astrometry using 4 common sources. We find a relative offset between the two coordinate frames (*Chandra* to Gemini) of $\delta\text{RA} = -0.06 \pm 0.21''$ and $\delta\text{Dec} = -0.01 \pm 0.17''$, leading to a refined X-ray afterglow position of RA=15^h35^m47.478^s, Dec=−28°46′56.30″ with an uncertainty of about 0.35″ radius that takes into account a centroid uncertainty of about 0.06″; see Figure 1). The *Chandra* position is in excellent agreement with the optical afterglow position.

2.3. Optical/Near-IR Host Galaxy Observations

In the second Gemini observation we detect an extended source near the afterglow position with $m_i = 24.80 \pm 0.15$ mag (including zero-point uncertainty and corrected for Galactic extinction) located at RA=15^h35^m47.477^s, Dec=−28°46′56.44″, with a centroid uncertainty of about 0.10″. We consider this source to be the host galaxy of GRB 120804A. Given the brightness of the galaxy, the probability of chance coincidence using a radius of 1″ (e.g., Bloom et al. 2002; Berger 2010) is $P_{\text{cc}} \approx 0.02$. We investigate potential association with brighter galaxies ($\approx 19–21$ mag) at larger offsets ($\approx 0.2–1'$) but find chance coincidence probabilities of $P_{\text{cc}} \approx 0.2–0.7$, indicating that these are not likely to be associated with GRB 120804A.

We also observed GRB 120804A with GMOS on the Gemini-North telescope on 2012 August 4.24 UT ($\delta t \approx 0.20$ d) in r -band with a total exposure time of 2340 s. We process the data using the `gemin` package in IRAF, and perform photometry using a zero-point of 28.41 ± 0.02 mag measured on the nights of July 27 – August 9 UT. Photometry at the position of the host galaxy reveals a faint source with $m_r = 26.2 \pm 0.2$ mag, corresponding to a flux density of $F_\nu = 0.19 \pm 0.04 \mu\text{Jy}$ (corrected for Galactic extinction). Since this was an early observation, the measurement may be contaminated by afterglow emission. However, taking into account a spectral shape of $F_\nu \propto \nu^{-0.6}$ and the large rest-frame extinction (see §3) we conclude that the afterglow contribution is sub-dominant, $\approx 0.03 \mu\text{Jy}$.

We observed the host galaxy in J -band with the FourStar near-IR camera on the Magellan/Baade 6.5-m telescope on 2012 August 28.98 UT with a total on-source time of 2390 s. We analyze the data using a custom pipeline in python, and perform photometry using common sources with the 2MASS catalog. The host galaxy has a measured brightness of $m_J = 23.05 \pm 0.20$ mag (corrected for Galactic extinction).

We obtained Y - and K_s -band observations with the High Acuity Wide-field K-band Imager (HAWK-I) on the VLT starting on 2012 September 7.96 UT, with a total exposure time of 1320 s in each filter. We produce dark-subtracted and flat-fielded images of the field using the HAWK-I pipeline within `esorex`, and perform photometry on the K_s -band image relative to the 2MASS catalog. We determine the Y -band calibration using the instrumental zero-point (appropriate for our observations, which were obtained in good conditions), and confirm that this is appropriate by extrapolating 2MASS J -band photometry to observations taken in the i -band. The host galaxy is detected in the K_s -band with $m_K = 22.0 \pm 0.1$ mag, and weakly in Y -band with $m_Y = 23.7 \pm 0.3$ mag (both values are corrected for Galactic extinction).

Finally, we obtained spectroscopic observations of the host galaxy with the FOCal Reducer and low dispersion Spectrograph (FORs2) on the VLT on 2012 August 19.01 UT. The observations consisted of 4×600 s exposures, covering the wavelength range 4300–9300 Å. We set the slit position angle to 149° to cover the host and nearby galaxy (see Figure 1). We detect no continuum or line emission at the position of the host galaxy, and only a faint continuum from the nearby galaxy.

The host galaxy photometry is summarized in Table 2. We also provide photometry for the extended source located $\approx 1.4''$ to the south-east of the host galaxy position (Figure 1).

2.4. Radio Observations

We observed GRB 120804A with the Karl G. Jansky Very Large Array (JVLA) starting on 2012 August 4.97 UT ($\delta t \approx 0.93$ d) at a mean frequency of 5.8 GHz. We utilized the WIDAR correlator (Perley et al. 2011b) with a bandwidth of about 1 GHz in each sideband, centered at 4.9 and 6.7 GHz. All observations were undertaken in the B configuration, utilizing 3C286 for bandpass and flux calibration, with interleaved observations of J1522–2730 for gain calibration. We calibrate and analyze the data using standard procedures in the Astronomical Image Processing System (AIPS; Greisen 2003), and list the resulting flux density measurements in Table 1.

In the first four epochs ($\delta t \approx 0.9$ – 10.9 d) we detect a single unresolved source coincident with the optical and X-ray afterglow, as well as the host galaxy: RA=15^h35^m47.485^s

(± 0.008), Dec= $-28^\circ 46' 56.44''$ (± 0.20). However, the source remains constant in brightness, with flux densities of $F_\nu(4.9 \text{ GHz}) = 43 \pm 4 \mu\text{Jy}$ and $F_\nu(6.7 \text{ GHz}) = 25 \pm 4 \mu\text{Jy}$. The steady brightness and optically thin spectrum, $F_\nu \propto \nu^{-1.7 \pm 0.8}$, are unprecedented for GRB radio afterglows at early time (Granot & Sari 2002), but are instead suggestive of emission from the host galaxy. Indeed, the centroid of the radio source shows a smaller offset relative to the optical host galaxy centroid ($0.10''$) than to the optical afterglow position ($0.28''$). The probability of chance coincidence for a source of this brightness within $\sim 1''$ of the optical/near-IR host galaxy position is $P_{\text{cc}} \approx 2 \times 10^{-4}$, based on the number counts of faint 5 GHz sources (Fomalont et al. 1991). This indicates that the radio source is the host galaxy of GRB 120804A. The observation on 2012 September 11 UT was obtained during a JVLA re-configuration leading to poorer noise characteristics in the resulting image. The 3σ limits are consistent with the earlier detections of the steady source.

We use the lack of variability to place a 3σ upper limit on the radio afterglow brightness of $F_\nu(5.8 \text{ GHz}) \lesssim 20 \mu\text{Jy}$.

In addition, we obtained JVLA observations of the LIRG host galaxy of GRB 100206A (Perley et al. 2011a) on 2012 September 10.27 UT to determine whether its large total star formation rate inferred from optical/IR data ($\sim 40 M_\odot \text{ yr}^{-1}$) produces radio emission. The observing setup and data analysis follow the procedure described above. We observed 3C48 for flux and bandpass calibration, and interleaved observations of J0238+1636 for gain calibration. There is a bright, contaminating source in the field (27 mJy at 4.9 GHz and 7 mJy at 6.7 GHz), located about $4.5'$ from the position of GRB 100206A. We therefore image the field utilizing self-calibration techniques on this bright source, leading to a non-detection of radio emission with a conservative 5σ limit of $F_\nu(5.8 \text{ GHz}) \lesssim 0.1 \text{ mJy}$.

3. AFTERGLOW PROPERTIES

We model the X-ray data, optical detection, and radio upper limits using the standard afterglow synchrotron model (Granot & Sari 2002). We follow the standard assumptions of synchrotron emission from a power-law distribution of electrons ($N(\gamma) \propto \gamma^{-p}$ for $\gamma \geq \gamma_m$) with constant fractions of the post-shock energy density imparted to the electrons (ϵ_e) and magnetic fields (ϵ_B). The additional free parameters of the model are the isotropic-equivalent blast-wave kinetic energy ($E_{\text{K,iso}}$), and the circumburst density (n for a constant density medium).

We note three key observational facts to guide the afterglow modeling. First, the X-ray light curve is best fit with a single decline rate of $\alpha_X = -0.93 \pm 0.06$, which coupled with the spectral index of $\beta_X \approx -0.9 \pm 0.1$ (§2.1) indicates that the synchrotron cooling frequency is $\nu_c \sim \nu_X$ and that $p \approx 2.2$. Second, the peak of the X-ray afterglow is ≈ 10 – $20 \mu\text{Jy}$ at $\delta t \approx 200$ s. This suggests that the radio light curve will eventually reach a similar peak flux density if the synchrotron peak frequency is $\nu_m \approx \nu_X$ at $\delta t \approx 200$ s. Such a peak flux density is consistent with our inferred radio upper limits. Finally, the optical and X-ray flux densities at $\delta t \approx 5.5$ hr are comparable, indicating that the optical to X-ray spectral index is $\beta_{\text{OX}} \approx 0$, compared to an expected slope of ≈ 0.6 (for $p = 2.2$ and $\nu_c \sim \nu_X$). This shallow slope indicates that GRB 120804A can be classified as a “dark” burst, following the definition of Jakobsson et al. (2004).

Guided by these results, we find that the data can be fit with the following parameters (using $z = 1.3$; see §4): $E_{\text{K,iso}} \approx$

8×10^{51} erg, $n \approx 10^{-3}$ cm $^{-3}$, $\epsilon_e \approx 0.3$, $\epsilon_B \approx 0.1$, and $p \approx 2.2$. The inferred blast-wave energy is comparable to the isotropic-equivalent γ -ray energy, $E_{\gamma,\text{iso}} \approx 6 \times 10^{51}$ erg. To explain the suppressed optical emission we also require $A_V^{\text{host}} \approx 2.5$ mag (at $z = 1.3$). The resulting light curves are shown in Figure 2. Models with higher values of $E_{K,\text{iso}}$ and/or n lead to a lower value of ν_m and a larger peak flux density, and therefore violate the radio limits (see for example dotted line in Figure 2).

In addition, the lack of a break in the X-ray light curve to at least ≈ 20 d places a lower bound on the jet collimation angle, with $\theta_j \gtrsim 8^\circ$, where we use the values of $E_{K,\text{iso}}$ and n inferred above. This indicates a beaming correction factor of $f_b^{-1} \equiv [1 - \cos(\theta_j)]^{-1} \lesssim 120$, and hence a beaming-corrected energy scale of $E_\gamma + E_K \approx 1.1 \times 10^{50} - 1.4 \times 10^{52}$ erg; the upper bound is set by isotropy.

Since in the afterglow model above, the X-ray light curve sets the overall flux density scale, an alternative explanation for the radio non-detections and the low optical flux density is that the X-ray emission is dominated by a different emission mechanism. One possibility is contribution from inverse Compton emission (Sari & Esin 2001), but this requires a large density of $n \gtrsim 10^2$ cm $^{-3}$. Another possibility is emission from a newly-born rapidly-spinning magnetar (e.g., Zhang & Mészáros 2001), but the expected evolution in this case is a relatively constant brightness for a duration similar to the spin-down timescale, followed by $F_\nu \propto t^{-2}$ at later time (for a typical braking index of 3). This is quite distinct from the observed single power law of $F_\nu \propto t^{-1}$ at $\delta t \gtrsim 200$ s.

4. A ULIRG HOST GALAXY

The observed optical/near-IR spectral energy distribution (SED) of the host galaxy exhibits a red color of $i - K \approx 2.8$ mag (≈ 4.3 Vega mag); the less certain $r - K$ color is ≈ 3.9 mag (≈ 5.6 Vega mag). There is also noticeable steepening between the i - and Y -band filters. These properties are indicative of a Balmer/4000 Å break at $z \approx 1.3$ (with a range of $\approx 1.1 - 1.5$) and either an old or dusty stellar population.

Taken in conjunction with the radio detection, the SED is reminiscent of ULIRGs ($L_{\text{FIR}} \gtrsim 10^{12} L_\odot$). To investigate this possibility we compare the host galaxy fluxes to the SED⁹ of the local ULIRG Arp 220. As shown in Figure 3, at $z \approx 1.3$ a simple scaling of Arp 220 provides a remarkable fit to the data. An elliptical galaxy template (2 Gyr old population; Polletta et al. 2007) at $z \approx 1.3$ provides a reasonable fit in the optical/near-IR (although it underestimates the observed r - and K_s -band fluxes), but cannot explain the radio emission (Figure 3).

At $z \approx 1.3$ the rest-frame B -band absolute magnitude is $M_B \approx -20.2$ mag, or $L_B \approx 0.2 L^*$ in comparison to the B -band luminosity function at $z \sim 1.3 - 2$ (Ilbert et al. 2005). The rest-frame K -band absolute magnitude is $M_K \approx -22.1$ mag (-24.0 Vega mag, or $L_K \approx 0.4 L^*$; Caputi et al. 2006b). This luminosity corresponds to a stellar mass of $M_* \times \approx 10^{10} M_\odot$ (using a characteristic mass-to-light ratio of $M_*/L_K \approx 0.3$; Drory et al. 2004). The infrared bolometric luminosity scaled using the SED of Arp 220 is $L_{\text{FIR}} \approx 10^{12} L_\odot$.

The unobscured star formation rate is inferred from the observed r -band ($\lambda_0 \approx 2700$ Å) to be $\approx 1 M_\odot \text{ yr}^{-1}$. However, from the observed radio emission we estimate the total star

formation rate to be much larger (Yun & Carilli 2002):

$$\text{SFR} \approx \frac{F_{\nu,\mu\text{Jy}} d_{L,\text{Gpc}}^2 / (1+z)}{25\nu_{0,\text{GHz}}^{-0.75} + 0.7\nu_{0,\text{GHz}}^{-0.1}} \approx 300 M_\odot \text{ yr}^{-1}, \quad (1)$$

where $\nu_0 = (1+z)\nu_{\text{obs}}$ is the rest frequency, and d_L is the luminosity distance. Assuming that the host stellar mass has been assembled with this star formation rate gives a characteristic age of about 0.15 Gyr. Using the limit on radio emission from GRB 100206A in Equation 1 we find $\text{SFR} \lesssim 60 M_\odot \text{ yr}^{-1}$.

The large star formation rate in the host of GRB 120804A is also expected to produce X-ray emission, with $L_X \approx 7 \times 10^{39} \times \text{SFR} \text{ erg s}^{-1}$ (Watson et al. 2004; Vattakunnel et al. 2012). For the values inferred above we find an expected luminosity of $L_X \approx 2 \times 10^{42} \text{ erg s}^{-1}$, corresponding to a flux of $F_X \approx 4.5 \times 10^{-16} \text{ erg s}^{-1} \text{ cm}^{-2}$. This is about 55 times lower than the afterglow flux measured with XMM-Newton at $\delta t \approx 19$ d, and hence consistent with a star formation origin for the radio emission.

An alternative interpretation of the radio detection is emission from an active galactic nucleus (AGN). Matching the standard template of a radio-quiet AGN (Shang et al. 2011) to the observed radio flux density (using $z = 1.3$), leads to a substantial over-estimate of the optical/near-IR brightness, and a much bluer color (Figure 3). Similarly, the expected X-ray flux in this scenario is $F_X \approx 6.4 \times 10^{-14} \text{ erg cm}^{-2} \text{ s}^{-1}$, several times brighter than the XMM-Newton detection of the afterglow. Thus, we can rule out a radio-quiet AGN origin. If we instead use the standard radio-loud AGN template (Shang et al. 2011) matched to the radio flux density, we find that the expected optical/near-IR and X-ray fluxes are $\sim 1 - 2$ orders of magnitude fainter than measured (Figure 3). Indeed, the observed lower bound on the ratio of radio to X-ray luminosity, $\nu L_{\nu,\text{rad}}/L_X \gtrsim 2 \times 10^{-4}$, along with an upper bound of $L_X \lesssim 5 \times 10^{44} \text{ erg s}^{-1}$ are in good agreement with samples of low-luminosity AGN (e.g., Terashima & Wilson 2003). In this scenario, the optical/near-IR emission is instead dominated by a stellar component, either from an old population or a reddened young population with a modest star formation rate of a few $M_\odot \text{ yr}^{-1}$.

While both a ULIRG and an AGN origin can explain the observed radio emission, we note that the former also offers a natural explanation for the inferred extinction, and fits the broad-band host SED with a single component. We therefore consider a ULIRG as the more likely explanation for the host galaxy of GRB 120804A.

The offset between the optical afterglow position and host galaxy centroid is $0.27 \pm 0.15''$, corresponding to 2.2 ± 1.2 kpc at $z \approx 1.3$. This is a relatively small offset for short GRBs (with a median of ≈ 5 kpc; Fong et al. 2010; Berger 2010), though not unprecedented. Still, in the context of a ULIRG origin, the small offset is consistent with the inferred afterglow extinction.

Finally, we determine a photometric redshift for the galaxy located $\approx 1.4''$ from the host galaxy position and find $z \approx 1.3$, consistent with that of the host galaxy (Figure 3). Thus, it appears likely that these galaxies, with a projected separation of about 11 kpc, are interacting or merging. This is not unexpected since at least some ULIRG activity is triggered by galaxy mergers.

5. SUMMARY AND CONCLUSIONS

We presented the discovery and sub-arcsecond localization of the optical and X-ray afterglow of the short GRB 120804A.

⁹ Obtained from the SWIRE Template Library (Polletta et al. 2007). We note that ULIRG templates exhibit some variability, but this will have little effect on the resulting photometric redshift.

A comparison of the observed fluxes points to substantial rest-frame extinction of $A_V^{\text{host}} \approx 2.5$ mag, commensurate with the large neutral hydrogen column density, $N_{\text{H,int}} \approx 2 \times 10^{22} \text{ cm}^{-3}$. In conjunction with deep radio limits we infer an energy of $E_{\gamma,\text{iso}} \approx E_{\text{K,iso}} \approx 7 \times 10^{51}$ erg and a low circumburst density of $n \sim 10^{-3} \text{ cm}^{-3}$. The lack of a break in the X-ray afterglow at $\lesssim 20$ d, leads to $\theta_j \gtrsim 8^\circ$, in line with existing measurements of short GRB jets (Fong et al. 2012). We note that a 60 ks *Chandra* observation obtained at $\delta t \approx 46$ d (PI: Burrows) may extend this limit to $\gtrsim 11^\circ$ if no break is detected (i.e., an expected flux of $\approx 7 \times 10^{-15} \text{ erg s}^{-1} \text{ cm}^{-2}$), or determine an angle of $\theta_j \approx 10^\circ$ if a break at an intermediate time of ≈ 33 d is detected (i.e., leading to an expected flux of $\approx 5 \times 10^{-15} \text{ erg s}^{-1} \text{ cm}^{-2}$). In either case, our estimate of $\theta_j \gtrsim 8^\circ$ will not change significantly.

We also detect the host galaxy of GRB 120804A, which exhibits red optical/near-IR colors and radio emission that are well-matched by the SED of a ULIRG (Arp 220) at $z \approx 1.3$. The inferred total star formation rate is $\approx 300 M_\odot \text{ yr}^{-1}$. A low-luminosity radio-loud AGN in an elliptical galaxy cannot be definitively ruled out, but the ULIRG interpretation, combined with the small projected offset of 2.2 ± 1.2 kpc, more naturally explains the inferred afterglow extinction. The host galaxy is part of an interacting/merging system, which is not unexpected for ULIRGs. Observations with the Atacama Large Millimeter/submillimeter Array (ALMA) will be able to robustly distinguish the two scenarios. At 240 GHz (ALMA band 6), the expected flux densities are about 0.3 mJy and 1 μJy , for the ULIRG¹⁰ and AGN cases, respectively. The former can be detected with high significance in a short observation. Similarly, the 60 ks *Chandra* observation at $\delta t \approx 46$ d can achieve a limiting flux of $F_X \approx 1.5 \times 10^{-15} \text{ erg s}^{-1} \text{ cm}^{-2}$, which is still about 3 times higher than the expected X-ray emission due to star formation. Therefore, if flattening of the X-ray light curve is detected in this observation, it may point to an AGN contribution.

The host galaxy of the short GRB 100206A at $z = 0.407$ is also a luminous infrared galaxy, $L_{\text{IR}} \approx 4 \times 10^{11} L_\odot$, with $\text{SFR} \approx 30\text{--}40 M_\odot \text{ yr}^{-1}$ inferred from SED fitting of data at $\sim 0.3\text{--}10 \mu\text{m}$ (Perley et al. 2011a). Here we find $\text{SFR} \lesssim 60 M_\odot \text{ yr}^{-1}$ from radio observations. Of the ≈ 25 short GRBs with robust host galaxy associations (Fong et al. in preparation), the hosts of GRBs 120804A and 100206A are the only galaxies with clear LIRG/ULIRG properties. At $z \sim 1$, the population of ULIRGs and bright LIRGs accounts for $\sim 25\%$

¹⁰ This flux density is relevant for the scaled SED of Arp 220. Variations in the dust temperature would lead to a range of potential flux densities (e.g.,

of the total star formation rate density (Le Flocc’h et al. 2005; Caputi et al. 2007), but their contribution to the stellar mass density is small, $\sim 1\text{--}few\%$ (e.g., Caputi et al. 2006a). Thus, the fraction of $\sim 5\text{--}10\%$ in the short GRB host population is intermediate between the star formation and mass weighted fractions. This is expected for a progenitor population that tracks both star formation and stellar mass, consistent with previous findings for short GRBs (Leibler & Berger 2010).

We thank Karina Caputi, Ranga Chary, Francesca Civano, Martin Elvis, and Jane Rigby for useful discussions about ULIRGs and AGN. We also thank Brian Metzger for information on the magnetar scenario. The Berger GRB group at Harvard is supported by the National Science Foundation under Grant AST-1107973, and by NASA/Swift AO7 grant NNX12AD69G. E.B. acknowledges partial support of this research while in residence at the Kavli Institute for Theoretical Physics under National Science Foundation Grant PHY11-25915. The Dark Cosmology Centre is funded by the Danish National Research Foundation. V. M. acknowledges funding through contract ASI-INAF I/004/11/0. Observations were obtained with the JVLA (program 12A-394) operated by the National Radio Astronomy Observatory, a facility of the National Science Foundation operated under cooperative agreement by Associated Universities, Inc. The paper includes data gathered with the 6.5 meter Magellan Telescopes located at Las Campanas Observatory, Chile; with ESO Telescopes at the La Silla Paranal Observatory under programme ID 089.D-0450; with the Gemini Observatory, which is operated by the Association of Universities for Research in Astronomy, Inc., under a cooperative agreement with the NSF on behalf of the Gemini partnership: the National Science Foundation (United States), the Science and Technology Facilities Council (United Kingdom), the National Research Council (Canada), CONICYT (Chile), the Australian Research Council (Australia), Ministério da Ciência, Tecnologia e Inovação (Brazil) and Ministerio de Ciencia, Tecnología e Innovación Productiva (Argentina). This work is based in part on observations obtained with XMM-Newton, an ESA science mission with instruments and contributions directly funded by ESA Member States and the USA (NASA).

Facilities: Swift (XRT), CXO (ACIS-S), XMM-Newton Gemini:North (GMOS), Magellan (FourStar), VLT (HAWK-I), JVLA

Yun & Carilli 2002; Michałowski et al. 2008).

REFERENCES

- Alard, C. 2000, *A&AS*, 144, 363
 Baumgartner, W. H., et al. 2012, GRB Coordinates Network, 13581, 1
 Berger, E. 2007, *ApJ*, 670, 1254
 Berger, E. 2009, *ApJ*, 690, 231
 Berger, E. 2010, *ApJ*, 722, 1946
 Berger, E. 2011, *New Astronomy Reviews*, 55, 1
 Berger, E., et al. 2007, *ApJ*, 664, 1000
 Berger, E., et al. 2005, *Nature*, 438, 988
 Bloom, J. S., Kulkarni, S. R., & Djorgovski, S. G. 2002, *AJ*, 123, 1111
 Burrows, D. N., et al. 2006, *ApJ*, 653, 468
 Caputi, K. I., Dole, H., Lagache, G., McLure, R. J., Dunlop, J. S., Puget, J.-L., Le Flocc’h, E., & Pérez-González, P. G. 2006a, *A&A*, 454, 143
 Caputi, K. I., et al. 2007, *ApJ*, 660, 97
 Caputi, K. I., McLure, R. J., Dunlop, J. S., Cirasuolo, M., & Schael, A. M. 2006b, *MNRAS*, 366, 609
 Chester, M. M., & Lien, A. Y. 2012, GRB Coordinates Network, 13582, 1
 Drory, N., Bender, R., Feulner, G., Hopp, U., Maraston, C., Snigula, J., & Hill, G. J. 2004, *ApJ*, 608, 742
 Eichler, D., Livio, M., Piran, T., & Schramm, D. N. 1989, *Nature*, 340, 126
 Fomalont, E. B., Windhorst, R. A., Kristian, J. A., & Kellerman, K. I. 1991, *AJ*, 102, 1258
 Fong, W., Berger, E., & Fox, D. B. 2010, *ApJ*, 708, 9
 Fong, W., et al. 2012, *ApJ*, 756, 189
 Granot, J., & Sari, R. 2002, *ApJ*, 568, 820
 Greisen, E. W. 2003, *Information Handling in Astronomy - Historical Vistas*, 285, 109
 Grupe, D., Burrows, D. N., Patel, S. K., Kouveliotou, C., Zhang, B., Mészáros, P., Wijers, R. A. M., & Gehrels, N. 2006, *ApJ*, 653, 462
 Hook, I. M., Jørgensen, I., Allington-Smith, J. R., Davies, R. L., Metcalfe, N., Murowinski, R. G., & Crampton, D. 2004, *PASP*, 116, 425
 Ibert, O., et al. 2005, *A&A*, 439, 863

- Jakobsson, P., Hjorth, J., Fynbo, J. P. U., Watson, D., Pedersen, K., Björnsson, G., & Gorosabel, J. 2004, *ApJ*, 617, L21
- Kalberla, P. M. W., Burton, W. B., Hartmann, D., Arnal, E. M., Bajaja, E., Morras, R., & Pöppel, W. G. L. 2005, *A&A*, 440, 775
- Le Floch, E., et al. 2005, *ApJ*, 632, 169
- Leibler, C. N., & Berger, E. 2010, *ApJ*, 725, 1202
- Margutti, R., Zaninoni, E., Bernardini, M. G., Chincarini, G., & for the Swift-XRT team. 2012, *ArXiv e-prints*
- Michałowski, M. J., Hjorth, J., Castro Cerón, J. M., & Watson, D. 2008, *ApJ*, 672, 817
- Nakar, E. 2007, *Phys. Rep.*, 442, 166
- Narayan, R., Paczynski, B., & Piran, T. 1992, *ApJ*, 395, L83
- Norris, J., Gehrels, N., & Barthelmy, S. D. 2012, *GRB Coordinates Network*, 13585, 1
- Nysewander, M., Fruchter, A. S., & Pe'er, A. 2009, *ApJ*, 701, 824
- Osborne, J. P., Beardmore, A. P., Evans, P. A., & Goad, M. R. 2012, *GRB Coordinates Network*, 13577, 1
- Perley, D. A., Modjaz, M., Morgan, A. N., Cenko, S. B., Bloom, J. S., Butler, N. R., Filippenko, A. V., & Miller, A. A. 2011a, *ArXiv e-prints*
- Perley, R. A., Chandler, C. J., Butler, B. J., & Wrobel, J. M. 2011b, *ApJ*, 739, L1
- Polletta, M., et al. 2007, *ApJ*, 663, 81
- Rowlinson, A., et al. 2010, *MNRAS*, 408, 383
- Sakamoto, T., et al. 2012, *GRB Coordinates Network*, 13614, 1
- Sari, R., & Esin, A. A. 2001, *ApJ*, 548, 787
- Schlafly, E. F., & Finkbeiner, D. P. 2011, *ApJ*, 737, 103
- Shang, Z., et al. 2011, *ApJS*, 196, 2
- Soderberg, A. M., et al. 2006, *ApJ*, 650, 261
- Sudilovsky, V., Elliott, J., & Greiner, J. 2012, *GRB Coordinates Network*, 13579, 1
- Terashima, Y., & Wilson, A. S. 2003, *ApJ*, 583, 145
- Troja, E., Sakamoto, T., Gehrels, N., Donato, D., & Racusin, J. L. 2012, *GRB Coordinates Network*, 13640, 1
- Vattakunnel, S., et al. 2012, *MNRAS*, 420, 2190
- Watson, D., Hjorth, J., Jakobsson, P., Pedersen, K., Patel, S., & Kouveliotou, C. 2004, *A&A*, 425, L33
- Watson, D., Hjorth, J., Jakobsson, P., Xu, D., Fynbo, J. P. U., Sollerman, J., Thöne, C. C., & Pedersen, K. 2006, *A&A*, 454, L123
- Yun, M. S., & Carilli, C. L. 2002, *ApJ*, 568, 88
- Zhang, B., & Mészáros, P. 2001, *ApJ*, 552, L35

TABLE 1
JVLA OBSERVATIONS

| Date (UT) | δt (d) | Frequency (GHz) | F_ν (μJy) |
|----------------|-------------------|--------------------|-------------------------------|
| 2012 Aug 4.97 | 0.93 | 4.9 | 44 ± 8 |
| | | 6.7 | 25 ± 7 |
| 2012 Aug 5.99 | 1.95 | 4.9 | 40 ± 8 |
| | | 6.7 | 26 ± 7 |
| 2012 Aug 8.02 | 3.98 | 4.9 | 45 ± 9 |
| | | 6.7 | 25 ± 8 |
| 2012 Aug 14.94 | 10.90 | 4.9 | 45 ± 10 |
| | | 6.7 | 24 ± 9 |
| 2012 Sep 11.01 | 37.97 | 4.9 | $< 40^a$ |
| | | 6.7 | $< 36^a$ |

NOTE. — ^a Limits are 3σ .

TABLE 2
OPTICAL AND NEAR-IR OBSERVATIONS OF THE HOST AND NEARBY GALAXY

| Filter | λ_{obs} (μm) | Host Galaxy | | Nearby Galaxy | |
|----------------------|---|---------------------------|--|---------------------------|--|
| | | AB Magnitude ^a | F_{ν} ^a (μJy) | AB Magnitude ^a | F_{ν} ^a (μJy) |
| <i>r</i> | 0.630 | 25.9 ± 0.2^b | 0.16 ± 0.04^b | 26.0 ± 0.2 | 0.15 ± 0.03 |
| <i>i</i> | 0.779 | 24.8 ± 0.15 | 0.44 ± 0.07 | 24.4 ± 0.1 | 0.63 ± 0.06 |
| <i>Y</i> | 1.021 | 23.7 ± 0.3 | 1.20 ± 0.40 | 23.0 ± 0.2 | 2.30 ± 0.46 |
| <i>J</i> | 1.235 | 23.0 ± 0.2 | 2.19 ± 0.44 | 22.4 ± 0.15 | 3.98 ± 0.60 |
| <i>K_s</i> | 2.146 | 22.0 ± 0.1 | 5.75 ± 0.58 | 21.8 ± 0.1 | 6.85 ± 0.69 |

NOTE. — ^a These magnitudes and flux densities have been corrected for Galactic extinction of $E(B-V) \approx 0.204$ mag (Schlafly & Finkbeiner 2011). ^b This value has been corrected for an expected afterglow contribution of ≈ 0.03 μJy .

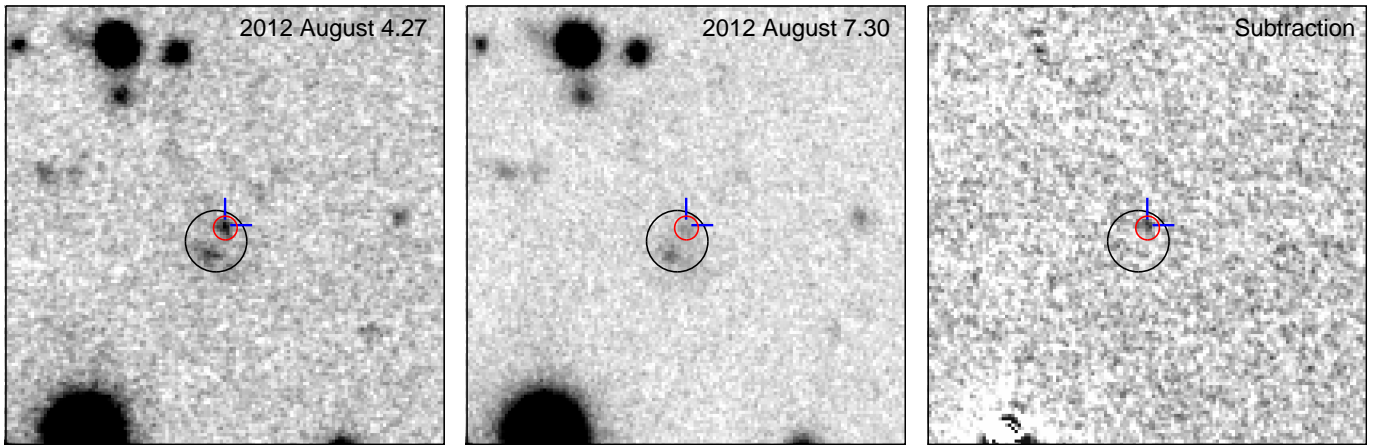


FIG. 1.— Gemini-North *i*-band images centered on the location of the *Swift*/XRT error circle (black circle; $1.4''$ radius 90% containment) obtained at $\delta t \approx 0.23$ d (left) and $\delta t \approx 3.26$ d (center), along with a subtraction of the two epochs (right). The subtraction reveals a fading optical afterglow (cross-hairs). The *Chandra* X-ray afterglow position coincides with the optical position (red circle; $0.54''$ radius 95% containment). Also seen is a galaxy located at a projected angular distance of $\approx 1.4''$ south-east of the host galaxy position. Each image is $20''$ on a side.

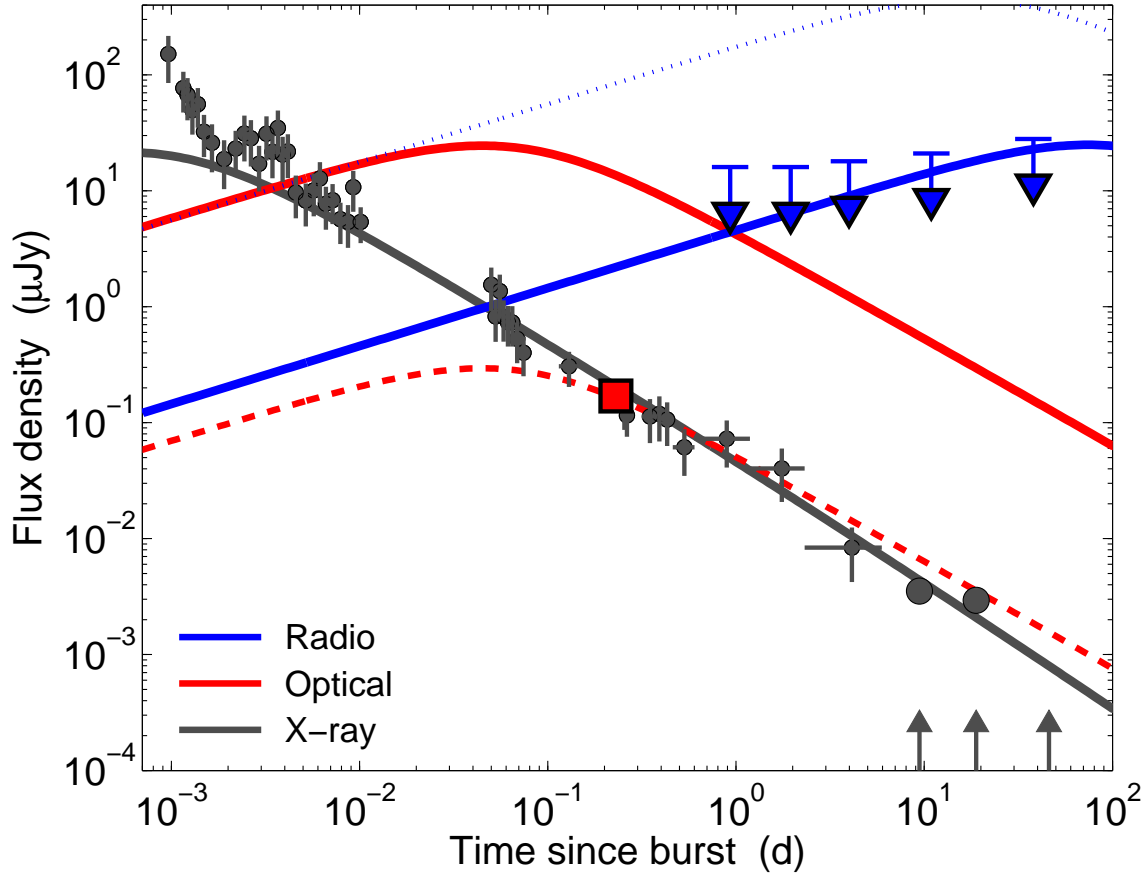


FIG. 2.— X-ray light curve, optical *i*-band detection, and radio 5.8 GHz upper limits for the afterglow of GRB 120804A. The solid lines are an afterglow model fit using the formulation of Granot & Sari (2002), with $E_{K,iso} \approx 8 \times 10^{51}$ erg, $n \approx 10^{-3}$ cm $^{-3}$, $\epsilon_e \approx 0.3$, $\epsilon_B \approx 0.1$, and $p \approx 2.2$. The low observed flux density in the optical band is suggestive of extinction, and can be explained with $A_V^{host} \approx 2$ mag (dashed red line). The dotted blue line indicates the predicted radio light curve for a model with fixed parameters of $n = 1$ cm $^{-3}$ and $E_{K,iso} = 6 \times 10^{51}$ erg (i.e., matched to $E_{\gamma,iso}$), that produces an indistinguishable fit in the X-rays (this model requires $\epsilon_e \approx 0.25$, $\epsilon_B \approx 0.1$, and $p \approx 2.1$). Clearly, such a high density can be ruled out. The arrows mark the *Chandra* and XMM-*Newton* observations, including the time of a late *Chandra* observation.

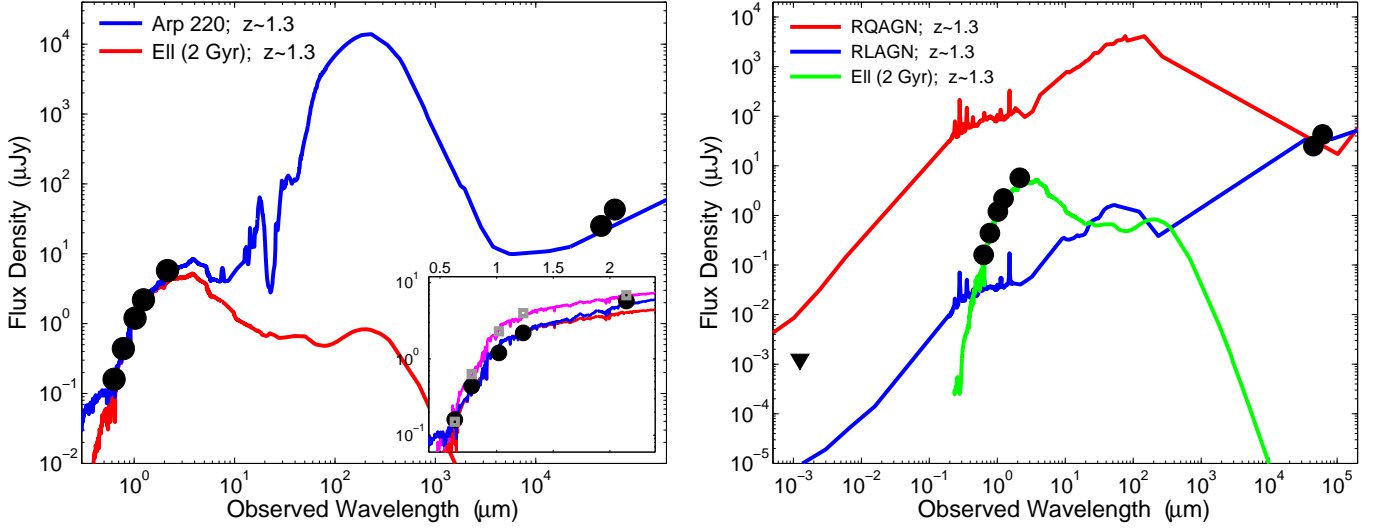


FIG. 3.— *Left:* Spectral energy distribution of the host galaxy of GRB 120804A (black circles: optical, near-IR, and radio) compared to a scaled SED of Arp 220 (blue line) and an elliptical galaxy with a 2 Gyr stellar population (red line) at $z = 1.3$. Both SEDs are scaled to match the optical/near-IR photometry of the host galaxy. The inset shows a zoom-in on the optical/near-IR range, highlighting that both SEDs provide a reasonable fit in this wavelength range (with a somewhat better fit in K_s -band for the Arp 220 SED). The gray symbols mark the photometry of the nearby galaxy, along with an elliptical galaxy model at $z = 1.3$. In both cases, the apparent steepening between the i - and Y -band filters points to a similar redshift. *Right:* Comparison to the scaled SEDs of radio-quiet (red line) and radio-loud (blue line) AGN at $z = 1.3$, as well as the SED of an elliptical galaxy with a 2 Gyr stellar population (green line). The AGN SEDs are scaled to match the observed radio flux density of the host galaxy. The radio-quiet AGN scenario over-predicts the optical, near-IR, and X-ray fluxes. On the other hand, the radio-loud scenario matches the radio flux density without violating the other measurements; the optical/near-IR emission is dominated by stellar emission.